Dual-Level Direct Dynamics Calculations of the Reaction Rates for a Jahn−Teller Reaction: Hydrogen Abstraction from CH_4 or CD_4 by $O(^3P)$

José C. Corchado,[†,‡] Joaquín Espinosa-García,[†] Orlando Roberto-Neto,[‡,§] Yao-Yuan Chuang,[‡] and Donald G. Truhlar*[,‡]

Departamento de Química Física, Universidad de Extremadura, 06071 Badajoz, Spain, and Department of Chemistry and Supercomputer Institute, University of Minnesota, Minneapolis, Minnesota 55455-0531

Received: January 28, 1998; In Final Form: April 10, 1998

We report calculations of the reaction rates of $O(^3P) + CH_4 \rightarrow OH + CH_3$ and $O(^3P) + CD_4 \rightarrow OD + CD_3$ over the temperature range 300−2500 K. The calculations are based on variational transition state theory in curvilinear coordinates with transmission coefficients calculated by the microcanonical optimized multidimensional tunneling approximation. A dual-level algorithm is used for the dynamical calculations. The higher level is UMP2/cc-pVTZ, and two lower levels are employed: PM3-SRP and an analytical potential energy surface. Using the canonical unified statistical model with microcanonical optimized multidimensional tunneling contributions, we obtain good agreement with experimental rate constants.

1. Introduction

Our ability to calculate reliable ab initio reaction rates by variational transition state theory has increased considerably in the past few years. This progress is due to the development of robust and economical methods for the quantitative treatment of reactions involving polyatomic systems with more than four atoms.[1] Included in the new methodological developments are schemes for carrying out dual-level direct dynamics[2,3] and methods to follow the reaction path with harmonic vibrational frequencies in curvilinear internal coordinates[4] and using redundant internal coordinates.[5] A critical issue for both the practicality and reliability of dynamics calculations is the method used for calculating potential energy surfaces (PESs). The cost of generating the necessary PES information is greatly reduced when one employs reaction-path dynamics methods[6] rather than full global dynamics. Such calculations can be based directly on ab initio or semiempirical electronic structure methods, in which case the potential energy surface is implicit,[1c] or on explicit analytical potential energy surfaces. A promising method for improving the effective level of the potential energy surface is dual-level direct dynamics.[1c,2,3] This approach involves the simultaneous use of two levels of calculations. A "lower level" is used at a large number of geometries to generate a whole PES, and a "higher level" is used at a few selected points, normally just the stationary points: reactants, products, and the saddle point. The "lower-level" (LL) PES may correspond to a post-Hartree−Fock method such as small-basis Møller−Plesset second-order perturbation theory[7] (MP2) or density functional theory,[8] semiempirical molecular orbital methods such as MNDO,[9] AM1,[10] or PM3,[11] NDDO-SRP[12] (neglect of diatomic differential overlap molecular orbital theory with specific reaction parameters), or an analytical potential energy function.[13]

In this article we apply dual-level dynamics and some of the new methods mentioned above to the study the reaction $CH_4 + O(^3P) \rightarrow CH_3 + OH$ and its CD_4 isotopomeric analogue. The $O(^3P) + CH_4$ reaction is a primary process in methane combustion and occurs by abstraction of a hydrogen by the oxygen.[14]

There is a large amount of experimental work on this reaction.[14−21] The most recent measurements, evaluated in ref 16, agree very well over the temperature range from 400 to 2500 K. Below 400 K the agreement is worse, due to uncertainties in the reaction stoichiometry[17] and possibly large tunneling effects[18] that make it dangerous to assume linear Arrhenius behavior. The recommended[16] expression for the rate constant for the temperature range 300−2500 K is[19]

$$k = 1.15 \times 10^{-15}\, T^{1.56} \exp(-4270/T)\ \mathrm{cm^3\ molecule^{-1}\ s^{-1}} \quad (1)$$

where T is in Kelvin. However, the expression 1 gives low-temperature rate constants lower than most of the experimental results.[16] Although Cohen[17a] proposes that experimental results tend to overestimate the low-temperature rate constants as a result of the above-mentioned uncertainties in the reaction stoichiometry, we think it is reasonable to also consider an alternative expression of the experimental results given by[17a]

$$k = 2.69 \times 10^{-18}\, T^{2.3} \exp(-3570/T)\ \mathrm{cm^3\ molecule^{-1}\ s^{-1}} \quad (2)$$

as it better represents the curvature in Arrhenius plots of the experimental data. Equation 2 leads to higher values of the rate constant than eq 1 at low temperatures (up to 60% higher at 300 K), in better agreement with the experimental values.

Despite the large amount of experimental work carried out on this reaction, there are just a few theoretical results. The reason could be that this reaction is particularly challenging because the approach of $O(^3P)$ along a C−H bond has 3-fold symmetry and leads to a Jahn−Teller conical intersection rather than a saddle point. The conical intersection corresponds to a ^3E state, and breaking the C_{3v} symmetry splits this into $^3A'$ and $^3A''$ surfaces.

[†] Universidad de Extremadura.
[‡] University of Minnesota.
[§] Permanent address: Instituto de Estudos Avançados, Centro Técnico-Aeroespacial, São José dos Campos, SP 12231-970, Brazil.

S1089-5639(98)00936-0 CCC: $15.00
Published on Web 05/28/1998

Walch and Dunning[22] carried out calculations of the classical barrier height and transition-state structure for the reaction $CH_4 + O(^3P)$ by employing a contracted basis set of the type [3s2p1d/2s1p] and using the polarization configuration interaction (Pol-CI) wave function method. Their calculated barrier height is 14.4 kcal/mol, and by comparison to similar calculations using the basis set [4s3p2d1f/3s2p1d] for the reaction $H_2 + O(^3P)$ they estimated a basis set error of 2.4 kcal/mol; with this correction their best estimate of the classical barrier height is 12.0 kcal/mol, and similarly they estimated 10.3 and 10.1 kcal/mol for the vibrationally adiabatic ground-state barrier height for the $^3A'$ and $^3A''$ states, respectively. The geometry of the transition state was located only approximately in their work because neither analytical nor numerical methods for the calculation of gradients or Hessians were available to search for the saddle point. In addition, the frequencies of the saddle point were estimated by treating the CH_3 group as if it were a point mass.

In a more recent article Gonzalez et al.[23] calculated the energies, structures, and harmonic frequencies for the reagents, products, and saddle point using second-order Møller−Plesset perturbation theory (MP2)[24] and fourth-order Møller−Plesset perturbation theory with projection (annihilation) of the spin contamination (PMP4). At the PMP4(SDTQ)/6-311G**//MP2/6-31G(d,p) level the classical barrier height was calculated to be 19.1 kcal/mol. We have to keep in mind that the Arrhenius expression does not provide a particularly good fit to the experimental data for this reaction and that, even when it does provide a good fit, Arrhenius activation energies provide only rough estimates of barrier heights; nevertheless, 19.1 kcal/mol is so much higher than the experimental values extracted from Arrhenius plots, for example, 8.7 kcal/mol[20] or 11.7 kcal/mol,[21] that it is unlikely to be correct. Gonzalez et al.[23] also calculated rate constants by conventional transition-state theory (TST) with Wigner's unidimensional method for tunneling contributions (TST/W); the calculated rate constants are in poor agreement with experiment due to the incorrect barrier height. When the rate constants are recalculated using Walch and Dunning's Pol-CI classical barrier of 12.0 kcal/mol, excellent agreement with the experimental rate constants is found. Gonzalez et al.[23] proposed that the reason for the overestimation of the barrier height at the PMP4(SDTQ)/6-311G**//MP2/6-31G(d,p) level could be the inadequacy of a single-configuration reference wave function for the post-Hartree−Fock calculations.

In this article we first calculate the energies, geometries, and frequencies of the reactants and products with several post-Hartree−Fock methods and with several basis sets to estimate the classical Born−Oppenheimer barrier height and the classical energy of the reaction. This set of electronic and structural results provides the higher-level calculations. In a second step we used and compared two different kinds of lower levels for the harmonic valley around the whole reaction path[6] and also for the wider reaction swath.[1b,25,26] In particular, we built an analytical potential energy surface (APS) and we determined a set of specific reaction parameters for the PM3 Hamiltonian, yielding what is called a PM3-SRP surface. One objective in using two different types of lower-level calculations here is to analyze the sensitivity of our predictions to the choice of the lower level, especially regarding the swath regions of the PES, which are important for calculating the large-curvature tunneling contributions and were not taken into account in the fitting of the SRP and APS parameters. To calculate the rate constants, we apply several variants of the dual-level dynamics method to perform variational transition state theory calculations with interpolated corrections (VTST-IC) calculations with inclusion of multidimensional tunneling effects.

2. Methods

2.1. Higher-Level Electronic Structure Calculations. The first step in the dual-level calculation is the determination of properties for the stationary points on the reaction path at the highest practical level. We calculated geometries, energies, and vibrational frequencies for the reactants, products, and saddle point. The first level chosen was second-order Møller−Plesset perturbation theory, MP2.[7,24] The MP2 wave function was based on both the unrestricted Hartree−Fock (UHF) wave function,[27] to be denoted as UMP2, and a restricted open-shell Hartree−Fock (ROHF) wave function,[28] to be denoted as ROMP2. Three basis sets were employed: 6-31G(d,p),[29] cc-pVDZ,[30] and cc-pVTZ.[30]

In some calculations, the contamination of the UMP2 wave function by undesired multiplet states was removed by using a projector operator.[31] The energies thus obtained will be denoted as PMP2. For comparison, some calculations were also performed using the coupled-cluster method involving single and double excitations and with perturbational treatment of the triple substitutions, CCSD(T),[32] based on the ROHF wave function [ROCCSD(T)]. Finally, we applied the scaling all correlation energy method (SAC)[33] to extrapolate the calculated energies of the reactants, products, and saddle point. This approach consists of scaling all the correlation energy, calculated as the difference between the Hartree−Fock (HF) and the post-Hartree−Fock (i.e., correlated) energies, by using a factor F, calculated as

$$F = \frac{D_e(\text{correlated}) - D_e(\text{HF})}{D_e(\text{exp}) - D_e(\text{HF})} \tag{3}$$

where "exp" denotes experimental. The SAC methods have been successfully used to compensate the deficiencies in the basis sets and in the treatment of electron correlation for several reactions,[34] and they are used here in our dual-level direct dynamics calculations.

Fully optimized geometries, harmonic vibrational frequencies, and zero-point vibrational energies (ZPVE) were calculated for the reactants, products, and saddle point. Electron correlation was included for both core and valence electrons. Six Cartesian d functions were used in all d sets, and 10 Cartesian f functions were used in the f sets. The ab initio electronic structure calculations were carried out using the GAUSSIAN 94 code[35] and the ACES II code[36] on IBM RS6000 model 550 and Silicon Graphics Power Challenge R8000 workstations.

2.2. Lower-Level Electronic Calculations. All three popular neglect-of-diatomic-differential-overlap (NDDO) methods, namely, MNDO, AM1, and PM3, were examined. An initial identification of the structure of the saddle point of the reaction $CH_4 + O(^3P)$ at the AM1 and PM3 levels of semiempirical molecular orbital theory was performed using the Berny algorithm[37] as implemented in GAUSSIAN 94.[35] Further refinement of the saddle point geometries as well as optimization of minima was carried out using version 5.07mn of the MOPAC code.[38] We developed a set of specific reaction parameters for the PM3 Hamiltonian that yield more accurate geometries and a more accurate endoergicity for this reaction than the original parameters. This level will be called PM3-SRP, and its specific reaction parameters, given in Table S-1 (tables numbered with an S prefix are in the Supporting Information), were adjusted by trial and error to give a physically balanced treatment of a

series of selected geometric and energetic properties. The structural and reactive properties used in the adjustment are classical barrier height, zero-point-inclusive saddle point barrier height ($\Delta V_a^{G,\ddagger}$), imaginary frequency of the saddle point, and Arrhenius activation energy calculated by a two-point fit at 300 and 2500 K. (The objective value for the last named quantity was 10.7 kcal/mol, as calculated from eq 1.)

2.3. Calibration of the Lower-Level Analytical Potential Energy Surface. As a second lower level we created an analytic function representing the potential energy for this reaction. We employed the same methodology as in previous work,[39] based on modifying the analytical PES proposed for a similar reaction. In particular we changed some parameters of the PES for the $CH_4 + H \rightarrow CH_3 + H_2$ reaction,[40] which is based on the analytic functions developed by Joseph et al.[41] and modified by Jordan and Gilbert.[42] The $CH_4 + H \rightarrow CH_3 + H_2$ reaction is a reasonable choice since, like the title reaction, it is a hydrogen abstraction reaction from methane to yield the CH_3 radical, with a slow change in geometry of the CH_3 group from pyramidal to planar during the reaction. Therefore, only minor changes were needed in order to fit the surface to selected data for the $CH_4 + O(^3P) \rightarrow CH_3 + OH$ reaction.

The first step in the refitting of the APS was to change the parameters related to the geometries, energies, and vibrational properties of the reactants and products, so that the endoergicity, geometries, and vibrational frequencies agree reasonably well with the available experimental values.[43] The following step was to refit some parameters in order to reproduce the characteristics of ab initio calculated saddle point: classical barrier height, geometry, and vibrational frequencies. Finally, the fit was required to reproduce reasonably well the experimental rate constants between 300 and 2500 K. The parameters modified from the analytical PES for the $CH_4 + H \rightarrow CH_3 + H_2$ reaction are listed in Table S-1. It should be noted that this fit was directed at obtaining a model analytical PES to serve in this work as a lower-level surface for the dual-level dynamics calculation, rather than as a stand-alone accurate reproduction of the available experimental and theoretical information.

2.4. Dynamics. The reduced mass used to scale all the coordinates[44] was set to 1 amu. This has no effect on calculated observables, but it does affect the magnitude of the reaction coordinate s when step sizes are specified and in plots used for interpretative purposes.

Dual-level dynamics calculations were performed using the two types of lower-level semiempirical PESs, in particular, using the new analytical potential surface and using the new semiempirical PES calculated at the PM3-SRP level.

The first step is to compute the minimum-energy path in isoinertial coordinates.[44−46] This is also called the IRC, and a variety of algorithms are available.[44−51] In the present calculations, the lower-level reaction path was computed using the Page-McIver method,[49] with a gradient step size of 0.005 a_0 and with the Hessian being recalculated every 4 steps. The reaction path was started by using a cubic expansion around the saddle point.[49] The abbreviation IC (interpolated corrections) is a generic term for the dual-level algorithms of refs 2 and 3; within this generic scheme, we employed two algorithms, interpolated-corrections-arithmetic[2] (ICA) and interpolated-corrections-logarithmic[3] (ICL) to interpolate corrections to the frequencies obtained from the two lower-level methods in order to study the sensitivity to the interpolation method. Note that the choice between ICA and ICL has no effect on the Born−Oppenheimer potential energy along the minimum-energy path. For the corrections to the energy we used both the Eckart-based correction[3] and the original formulation.[2] We also checked the effect of using a direct IVTST-0[52] interpolation for the modes corresponding to the two lowest frequencies (almost degenerate C−H−O bendings). The reaction path was calculated from −3.00 a_0 on the reactants side to 4.00 a_0 on the product side.

The rate constants are calculated using canonical variational (CVT) and the canonical unified statistical model (CUS),[53,54] which is a generalization of the earlier microcanonical unified statistical model.[55] The CVT method involves calculating the standard-state-generalized transition-state (GT) free energy of activation profile defined by

$$\Delta G^{GT,0}(T,s) = RT\left[\frac{V_{MEP}(s)}{kT} - \ln\frac{Q^{GT}(T,s)}{\phi^R(T)K^0}\right] \qquad (4)$$

where R is the gas constant, k is the Boltzmann constant, $Q^{GT}(T,s)$ is the partition function for a generalized transition state at a distance s along the minimum-energy path (MEP) from the saddle point, defined as positive in the product side and negative in the reactant side, and $V_{MEP}(s)$ is its potential energy; K^0 is the reciprocal of the standard-state concentration, and $\phi^R(T)$ is the reactant partition function per unit volume. In calculating electronic partition functions, we included the spin−orbit splitting of $O(^3P)$, which is 158.26 cm^{-1} and 226.98 cm^{-1} for $^3P_1$ and $^3P_0$ relative to $^3P_2$. We also included the two electronic states for the OH product in the calculations of its electronic partition functions, with a 140 cm^{-1} splitting. As a consequence of the electronic degeneracy (Jahn−Teller effect[56]), the potential energy surface for the $CH_4 + O(^3P)$ reaction splits into two surfaces of respective symmetries 3A′ and 3A″. Since our calculations are based on only the lowest surface, but the two surfaces make almost equal contributions to the rate, the electronic partition coefficients of the triplet ground-electronic-state generalized transition states are multiplied by 2, yielding an overall value of 6.

The variational transition state is optimized by finding the value $s = s(T)$ at which $\Delta G^{GT,0}$ is a maximum, and the CVT rate constant is defined by

$$k^{CVT}(T) = \sigma\frac{kT}{h}K^0 \min_s \exp[-\Delta G^{GT,0}(T,s)/kT] \qquad (5)$$

where σ is the reaction path symmetry factor, which is obtained by counting the number of equivalent reaction paths. Since the O atom can abstract four different H atoms, the value of σ for the forward reaction was taken as 4, while for the reverse reaction it is 2, since the OH radical can approach the C atom with the same probability on both faces of the planar CH_3 group.

Tunneling corrections are included as a mutiplicative factor, the ground-state transmission coefficient $\kappa^{tun}(T)$,

$$k^{CVT/tun}(T) = \kappa^{tun}(T)\, k^{CVT}(T) \qquad (6)$$

We consider four levels of tunneling corrections, zero-curvature tunneling (ZCT),[44,45] centrifugal-dominant small-curvature tunneling (SCT),[57] large-curvature tunneling (LCT),[26,53,57,58] and microcanonical optimized multidimensional tunneling (μOMT).[26] For the LCT calculation, the LCG3 version[57,58] of this approach was used, allowing the system to reach all energetically accessible excited vibrational product bound modes into which tunneling proceeds. Rotations are treated by the classical rigid rotor approximation, and vibrations are treated as quantum mechanical separable harmonic oscillators, with the generalized normal modes[53] defined in redundant curvilinear coordinates,[4,5,59] although, as indicated below, some

TABLE 1: Theoretical Equilibrium Bond Energies, D_e (kcal/mol), and F Parameters for the Species CH_4 and OH

	$CH_4 \rightarrow CH_3 + H$		$OH \rightarrow O + H$	
method	D_e	F	D_e	F
UMP2/cc-pVDZ	108.8	0.87	94.3	0.71
PMP2/cc-pVDZ	107.6	0.83	94.5	0.71
UMP2/cc-pVTZ	112.3	0.98	103.9	0.93
PMP2/cc-pVTZ	111.0	0.94	104.0	0.94
ROMP2/cc-PVTZ	112.0	0.97	104.0	0.93
ROCCSD(T)/cc-pVTZ	113.0	1.01	103.7	0.93
expt	112.7[a]		106.5[b]	

[a] Ref 33a. [b] Refs 43, 63.

testing was done using rectilinear[6a,6b,53,60] coordinates. The chosen curvilinear coordinates were all the possible bonds lengths and bond angles, including the C−H−O bend, which was treated as a degenerate bend.

For comparison, single-level dynamics were carried out using APS.

All dynamical calculations involving the PM3-SRP lower-level PES were carried out using the MORATE code, version 7.8,[58,61] which is an interface between the MOPAC 5.07mn[38] and the POLYRATE 7.8[57,62] codes. Both single-level and dual-level dynamical calculations involving the APS were performed using POLYRATE 7.8.[57,62] The calculations were carried out on IBM RS6000 model 550 and Silicon Graphics Power Challenge R8000 workstations and on a CRAY C90 supercomputer.

3. Results and Discussion

3.1. Structural and Energetic Properties. The bond dissociation energies of the reactants and products, CH_4 and OH, were obtained at UMP2, PMP2, ROMP2, and ROCCSD(T) levels, and using either the cc-pVDZ or cc-pVTZ basis set or both. The theoretical and experimental[33a,43,63] dissociation energies and the values of scaling factors F computed from eq 3 are shown in Table 1. The scaling factors are generally larger for the C−H bond than for the O−H bond. The UMP2 and PMP2 levels of calculation with the cc-pVDZ basis are particularly unbalanced. Notice that the PMP2/cc-pVTZ method has the best correlation balance with F values of 0.94 for both O−H and C−H bonds. Also, UMP2 is better balanced than ROCCSD(T). Overall, these F factors are not surprising since a value of roughly 0.8 has been stated to be typical.[64]

The reasonable performance achieved using the UMP2 approach for the present problem may result from error cancellation. A particularly important issue in the present case is that the reactants and products of the reaction suffer spin contamination by higher multiplet states with values of the operator $\langle S^2 \rangle$ being 2.047, 0.76, and 0.77 for the oxygen, hydroxyl, and methyl radicals, respectively, calculated at UMP2 level, as compared to exact values of 2.0, 0.75, and 0.75, respectively. The unbalanced results obtained at the ROCCSD(T)/cc-pVTZ level with the scaling factor F equal to 1.01 and 0.93 for the C−H and O−H bonds, respectively, may be explained by the fact that the ROHF reference functions do not suffer from spin contamination, but at the correlated level there is no guarantee that the wave function is a spin eigenfunction. This is true even when using the complete spin-adapted treatment.[32g] Thus, the best balance is obtained by using the PMP2/cc-pVTZ level; this will be the level that we will use for performing our SAC calculations.

The optimized geometries and the harmonic vibrational frequencies of OH, CH_3, and CH_4 using the AM1, PM3, PM3-SRP, APS (analytical potential surface), MP2, and ROCCSD(T) methods are listed in Tables 2 and 3, respectively. In both tables we also list experimental values[43] for comparison. Convergence of the calculations in reproducing the experimental geometries and frequencies is very slow in the case of the CH_4 molecule. The theoretical difficulty of describing methane quantitatively was discussed recently by Colt and Scuseria,[65] who achieved very good accuracy in the theoretical calculations when using the RCCSD(T) method and basis sets of polarized quadruple-ζ quality. At the semiempirical level of calculation there is an impressive improvement in the values of the geometries and of the frequencies when using specific reaction parameters. In the case of the values obtained with the APS method, the agreement is not surprising, since the empirical parameters of the analytical surface were adjusted to reproduce as close as possible the experimental reactants and products frequencies. All the harmonic vibrational frequencies calculated by the methods, PM3-SRP and APS, that we will use as lower levels in dual-level dynamics calculations agree with experiment within 5%, and the ZPVEs calculated by these methods agree with experiment within 4%.

Next we consider the saddle point, for which we performed a more detailed analysis than was done in previous studies.

When the O(^{3}P) atom approaches the CH_4 along a C−H axis with 3-fold symmetry, we obtain a symmetry of ^{3}E for the six-body system. In this case, according to the Jahn−Teller theorem,[56] the potential energy will not have a stationary point on the axis of symmetry, but rather there will be three equivalent stationary points with the oxygen off the C−H axis because the non-totally symmetrical normal coordinate corresponding to this displacement causes a splitting of the electronic state. This bending splits the ^{3}E state into two electronic states of symmetries ^{3}A′ and ^{3}A″. The geometrical structure of the saddle point, CH_4O, is shown in Figure 1.

Before examining the energies along the bending coordinate, we first searched for the saddle points at the UMP2/6-31G(d,p) level. (Transition-state structures corresponding to the ^{3}A′ and ^{3}A″ states were characterized previously by Gonzalez et al.[23]) In the present work we found that the ^{3}A′ and ^{3}A″ transitions states were almost identical in energy but differ slightly in the O−H−C bending angle; the saddle point geometries are given in Table 4. We also found two stationary points at the UMP2 level using the cc-pVDZ and cc-pVTZ basis sets. At the UMP2/cc-pVTZ level, the ^{3}A″ transition state has only one imaginary frequency; however, for the ^{3}A′ case two imaginary frequencies are present, with values of 2130i and 64i cm^{-1}. A UMP2/cc-pVDZ calculation also yields two imaginary frequencies for the stationary point located on the ^{3}A′ surface. Similar results were found by Kreye[66] in a UMP2/6-311G(d,p) study of the reaction of CHF_3 and O(^{3}P), where a stationary point was found on the ^{3}A′ surface with two imaginary frequencies with values 2645i and 87i cm^{-1}.

To get a clearer view of the bending curves of the ^{3}A″ and ^{3}A′ surfaces, we have carried out electronic calculations at the UMP2/6-31G(d,p) level varying the angle between O, H, and C in relation to a structure with a linear C−H−O angle at fixed internuclear distances, d(H−C) and d(H−O) (see Figures 1 and 2). The calculations of the PES from +30° to −30° were carried out in C_s symmetry (where the electronic states have ^{3}A″ and ^{3}A′ symmetry). The calculated PES (Figure 2) is very flat, and in the region of +10° to −10° the difference in energy between the ^{3}A″ and ^{3}A′ electronic PES is less than 0.1 kcal/mol. One consequence of this flat potential is that for a fully quantitative treatment anharmonicity of the corresponding large-amplitude

TABLE 2: Optimized Bond Lengths (in Å)

	AM1	PM3	PM3-SRP	APS	UMP2/ cc-pVDZ	UMP2/ cc-pVTZ	ROMP2/ cc-pVTZ	ROCCSD(T) cc-pVTZ	expt[a]
OH	0.949	0.937	0.987	0.971	0.974	0.966	0.966	0.970	0.971
CH_3	1.086	1.072	1.075	1.094	1.089	1.069	1.069	1.073	1.079
CH_4	1.112	1.087	1.091	1.070	1.098	1.080	1.080	1.082	1.091

[a] Ref 43.

TABLE 3: Harmonic Normal-Mode Vibrational Frequencies (in cm^{-1}) and Zero-Point Vibrational Energies, ZPVE (in kcal/mol), for the Species CH_4, CH_3, and OH and for the $^3A''$ Saddle Point

	mode	AM1	PM3	PM3- SRP	APS	UMP2/ cc-pVDZ	UMP2/ cc-pVTZ	ROMP2/ cc-pVTZ	ROCCSD(T)/ cc-pVTZ	expt[a]
OH	σ	3616	3988	3682	3735	3794	3822	3817	3745	3735
	ZPVE	5.2	5.9	5.3	5.3	5.4	5.5	5.5	5.4	5.3
CH_3	a_1	3252	3183	3133	3022	3185	3211	3207	3156	3002
	a_2	780	637	583	580	388	528	571	179	580
	e	3249	3272	3223	3188	3390	3372	3368	3308	3184
	e	1348	1263	1257	1257	1430	1442	1440	1411	1383
	ZPVE	19.1	18.8	18.1	18.2	18.9	19.1	19.1	18.3	18.2
CH_4	a_1	3216	3312	3256	2718	3090	3117	3117	3085	2916
	e	1412	1452	1444	1549	1571	1595	1595	1579	1534
	t_1	3189	3208	3153	3042	3241	3231	3231	3180	3018
	t_1	1380	1363	1362	1329	1342	1352	1352	1346	1306
	ZPVE	27.9	28.5	28.1	27.1	28.6	28.7	28.7	28.3	27.1
$OHCH_3$	ν_1	3190	3245	3176	3012	3302	3295	3287		
	ν_2	3131	3221	3171	3012	3286	3267	3270		
	ν_3	3131	3221	3171	2881	3134	3160	3158		
	ν_4	1400	1358	1338	1434	1448	1468	1472		
	ν_5	1374	1358	1338	1434	1422	1419	1425		
	ν_6	1374	1260	1191	1245	1217	1239	1245		
	ν_7	1230	1152	1004	1157	1099	1174	1175		
	ν_8	1221	1139	989	1157	1049	1168	1227		
	ν_9	905	665	471	597	606	628	668		
	ν_{10}	138	315	338	325	324	425	425		
	ν_{11}	128	312	333	325	320	218	190		
	ν_{12}	1486i	2304i	2532i	1507i	2145i	2130i	2582i		
	ZPVE	24.6	24.7	23.6	25.9	24.6	24.9	25.1		

[a] Ref 43.

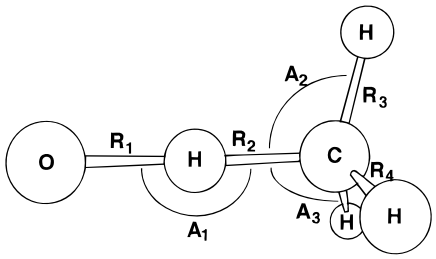

Figure 1. Geometrical parameters of the $CH_4 + O(^3P)$ saddle point.

vibration should probably be treated by a specialized method such as the rigid or semirigid bender approach,[67] although we will not extend the present calculations to that level, nor will we include Born−Oppenheimer breakdown[56b,68] terms.

The bending is very flat around the origin; thus the average position of the oxygen atom will be very close to the C_{3v} symmetry axis. The similarity between both curves and between the geometries and frequencies of the two saddle points allows us to assume that the dynamics for both $^3A'$ and $^3A''$ surfaces will be very similar. Thus, as mentioned above, we calculate the rate constant for the whole reaction as twice the rate constant for one of the surfaces. In particular, we calculate saddle point properties (Tables 3 and 5) and rate constants for the $^3A''$ surface, and we multiply them by 2 in order to obtain the rate constants for the $CH_4 + O(^3P)$ reaction. Note that the total reactive flux through the generalized transition state dividing surface is not expected to be very sensitive to the extent of nonadiabatic dynamical transitions between the two surfaces.

The saddle point geometries obtained at various levels are given in Table 5. The finding of conflicting predictions of the relative order of the lengths of the breaking C−H bond, R_2, and the forming O−H bond, R_1, is troublesome. At the UMP2 level using the 6-31G(d,p), cc-pVDZ, and cc-pVTZ basis sets, and at the Pol-CI level with a polarized double-ζ basis set, the bond length R_2 is greater than R_1, but the ROMP2/cc-pVTZ calculation gave the opposite order. The calculations at PM3-SRP, UMP2/cc-pVTZ, and ROMP2/cc-pVTZ levels indicate that the transition state has an early barrier with 15%, 14%, and 11% stretching of the H−C bond (as compared to the H−C bond in isolated methane) and 20%, 20%, and 22% stretching of the O−H bond (as compared to the H−O length in isolated OH). The greater elongation of the forming bond than the elongation of the breaking C−H indicates an early transition state. The APS calculations predict 16% stretching of the C−H bond and 12% stretching of the O−H bond; so there is a qualitative prediction of a nearly symmetrical barrier.

Table 6 summarizes the energetics at various levels. The SAC calculations are carried out using the scaling factor $F = 0.94$ (see Table 2) to scale the energies obtained at the PMP2/cc-pVTZ level. The classical forward barrier at this level is 14.0 kcal/mol, and including harmonic zero-point vibrational energy (ZPVE) reduces the forward barrier to 10.2 kcal/mol, which is within the range of experimental values of the activation energy (8.7−11.7 kcal/mol)[14] and in excellent agreement with the Pol-CI and APS results. There is also excellent agreement between our scaled calculations (PMP2-SAC/cc-pVTZ//UMP2/cc-pVTZ) and the experimental measurements of

TABLE 4: Comparison between Selected Properties of $^3A'$ and $^3A''$ Stationary Points at Different Levels of Calculation[a]

method	state	R_1 O−H	R_2 C−H	R_3 C−H	R_4 C−H	A_1 O−H−C	A_2 H−C−H	A_3 H−C−H	imaginary frequencies	energy[b]
UMP2/6-31G**[c]	3A′	1.179	1.289	1.082	1.081	181.05	103.9		2197i	19.12
	3A″	1.179	1.289	1.081	1.081	177.95	104.9		2188i	19.12
UMP2/cc-pVDZ	3A′	1.175	1.301	1.095	1.094	180.85	103.8	104.5	222i, 2146i	21.92
	3A″	1.175	1.301	1.094	1.095	178.35	104.7	104.0	2145i	21.92
UMP2/cc-pVTZ	3A′	1.201	1.250	1.077	1.076	180.66	103.9	104.5	64i, 2130i	17.84
	3A″	1.201	1.250	1.076	1.076	179.18	104.6	104.1	2130i	17.84

[a] Bond lengths are given in angstroms, angles in degrees, and frequencies in cm^{-1}. [b] Relative to reactants, kcal/mol. [c] Ref 23. Energies calculated at the PUMP4SDTQ/6-311G**//UMP2/6-31G** level. Note that 6-31G** and 6-31G(d,p) denote the same basis set.

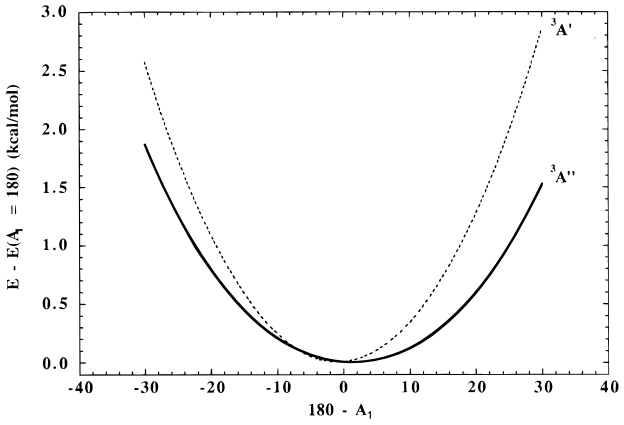

Figure 2. Energy profile for the $^3A'$ and $^3A''$ potential energy curves as function of the deviation from linearity of the C−H−O angle. For these calculations the other internal coordinates were fixed at the values $R_1 = 1.173$, $R_2 = 1.294$, $R_3 = 1.087$, $R_4 = 1.087$, $A_2 = 104.64$, $A_3 = 104.89$ for the $^3A'$ surface and $R_1 = 1.173$, $R_2 = 1.294$, $R_3 = 1.087$, $R_4 = 1.087$, $A_2 = 104.83$, $A_3 = 104.15$ for the $^3A''$ surface. The calculated energy of both structures with a linear C−H−O angle is 16.2 kcal/mol measured with respect to $O(^3P) + CH_4$.

ΔH_0^0, which could be expected from the method used for calculating the F factor.

In the case of the NDDO calculations with standard parameters there is an increasing improvement from the MNDO to the AM1 to the PM3 Hamiltonian when we compare the values of the forward classical barrier height and of the energies of the reactions (see Tables 5, 6, and S-2). All three methods predict too large of a forward classical barrier and a wrong sign for the energy of the reaction. When the PM3 parameters were adjusted (Table S-1), we successfully found better estimates of the classical barrier and a correct prediction of the sign of the endoergicity of the reaction. The analytical potential energy surface (APS) was adjusted using the experimental frequencies of the reactants and products, geometrical structures of the saddle point calculated at UMP2/6-31G(d,p), and the experimental data on the rate constants; as a result, the energies predicted using APS are in good agreement with experimental values.

3.2. Dual-Level Dynamics. Once we have determined the higher-level properties of the reactants, products, and saddle point, we carry out a dynamical calculation at the lower level but corrected by interpolated corrections[2,3] based on higher-order optimizations in order to obtain higher-level accuracy. According to the standard notation[69] for dual-level dynamics, these dual-level calculations are labeled as PMP2-SAC/cc-pVTZ//UMP2/cc-pVTZ///PM3-SRP and PMP2-SAC/cc-pVTZ //UMP2/cc-pVTZ///APS, when using as the lower level the semiempirical PM3-SRP surface and the analytical potential surface, respectively. However, in the rest of this paper we will use the simpler notations PM3-SRP-IC and APS-IC, respectively, since there is no possibility of confusion. Note that the interpolated corrections involve energies computed via geometry optimization at a higher level; this is a critical part of /// calculations (as compared to // calculations, which involve only energy corrections computed at the lower-level geometries).

We will start by examining the sensitivity to details of performing a dual-level calculation. First, we check the two available approximations for correcting the energy along the reaction path, $V_{MEP}(s)$. In the original formulation[2] the correction ΔV to the lower-level $V_{MEP}(s)$ was done by fitting the corrections at reactants, products, and saddle point to an Eckart function. In the improved method[3] the correction is approximated by the difference between two Eckart functions: one fitted to the lower-level $V_{MEP}(s)$, and the other one fitted to the higher-level energies for reactants, products, and saddle point and the imaginary frequency at the saddle point. The higher-level imaginary frequency was not used in the original formalism, but it is included in the improved method, and that apparently[3] allows us to get a better approximation of the shape of the higher-level $V_{MEP}(s)$, at least in the vicinity of the saddle point.

In Figure 3 we show the results of the two correction algorithms for the PM3-SRP surface. In Figure 4 we show the results for the APS surface. When using the PM3-SRP surface as the lower level, the two correction algorithms give very similar results. However, when the lower level is the APS surface, the two results differ greatly. In fact, the "improved" method seems to behave very badly in this case, leading to a significant well on each side of the barrier. The result can be understood by considering the imaginary frequency of the saddle point (Table 3) and the classical barrier height (Table 6). Both the original and improved IC methods correct the energy of the saddle point, but only the improved method uses the higher-level saddle point imaginary frequency to try to improve the barrier shape.

The higher-level imaginary frequency is 2130i cm^{-1}, and the barrier height is 14.0 kcal/mol. The PM3-SRP barrier height has to be lowered by 5 kcal and made broader, since the imaginary frequency has to be reduced by about 20%, which is reasonable since lower barriers are usually broader and have lower imaginary frequencies. Thus, both the original method and the improved method succeed in making the barrier wider and reducing its height, giving very similar shapes. However, when we use the APS as the lower level, the barrier height has to be slightly increased, by 0.4 kcal/mol. The small change in the barrier height leads the original method to predict a higher-level $V_{MEP}(s)$ almost parallel to the lower-level $V_{MEP}(s)$; the shape remains practically unchanged. Nevertheless, when we use the improved method, we also have to take into account that the imaginary frequency is about 30% larger at the higher level of calculation. The improved method tries to make the barrier thinner than the lower-level one, while its height remains almost unchanged. As a result, the barrier drops rapidly near the saddle point, leading to wells on both sides of the reaction path. The rapid drop is probably correct in the first few tenths

TABLE 5: Geometrical Structures of the $^3A''$ Saddle Point with C_s Symmetry[a]

method	R_1 O−H	R_2 C−H	R_3 C−H	R_4 C−H	A_1 O−H−C	A_2 H−C−H	A_3 H−C−H
MNDO	1.295	1.233	1.098	1.098	180.00	106.3	106.3
AM1	1.357	1.194	1.107	1.107	179.96	106.4	106.4
PM3	1.297	1.205	1.082	1.082	179.90	106.0	105.9
PM3-SRP	1.232	1.277	1.084	1.084	179.88	104.7	104.7
APS	1.104	1.319	1.095	1.095	180.00	107.6	107.6
Pol-CI[b]	1.20	1.36					
UMP2/6-31G(d,p)[c]	1.179	1.289	1.081	1.081	177.95	104.9	
UMP2/cc-pVDZ	1.175	1.301	1.094	1.095	178.35	104.7	104.0
UMP2/cc-pVTZ	1.201	1.250	1.076	1.076	179.18	104.6	104.1
ROMP2/cc-pVTZ	1.242	1.211	1.077	1.076	179.88	104.7	105.5

[a] Bond lengths are given in angstroms and angles in degrees. [b] Ref 22. [c] Ref 23.

TABLE 6: Energetic Properties (in kcal/mol) of the Reaction $CH_4 + O \rightarrow CH_3 + OH$

	forward reaction				reverse reaction	
method	$\Delta V^{\ddagger}$ *a*	$\Delta V_a^{G,\ddagger}$ *b*	ΔV *c*	ΔH_0^0 *d*	$\Delta V^{\ddagger}$ *a*	$\Delta V_a^{G,\ddagger}$ *b*
MNDO	27.4	20.7	−22.8	−26.1	50.2	46.8
AM1	11.4	8.1	−20.2	−23.8	31.6	31.9
PM3	10.8	7.0	−15.7	−19.5	26.5	7.0
PM3-SRP	19.0	14.6	6.5	1.8	12.5	12.8
APS	13.6	10.2	4.9	1.4	8.9	8.8
Pol-CI	12.0	10.2	8.5			
PMP4/6-31G**[e]	19.1	15.3	11.3	6.9	7.8	8.4
UMP2/cc-pVDZ	21.9	17.9	14.5	10.3	7.4	7.6
PMP2/cc-pVDZ[f]	18.9	14.9	13.1	8.9	5.8	6.0
ROMP2/cc-pVTZ	17.1	13.5	8.0	3.9	9.1	9.6
UMP2/cc-pVTZ	17.8	14.0	8.4	4.3	9.4	9.8
PMP2/cc-pVTZ[g]	15.1	11.3	7.0	2.9	8.0	8.4
PMP2-SAC/cc-pVTZ[g]	14.0	10.2	6.5	2.4	7.5	7.8
expt[h]			6.2	2.6		

[a] Born−Oppenheimer $^3A''$ barrier height. [b] Enthalpy of activation at 0 K evaluated at the 3A″ saddle point ($\Delta V_f^{\ddagger} + \Delta$ZPVE). [c] Born−Oppenheimer reaction energy. [d] Enthalpy of reaction at 0 K ($\Delta V +$ ΔZPVE). [e] PUMP4SDTQ/6-311G**//UMP2/6-31G**, from ref 23. [f] Single-point calculation at the UMP2/cc-pVDZ geometry. [g] Single-point calculation at the UMP2/cc-pVTZ geometry. [h] refs 33a, 43, 63.

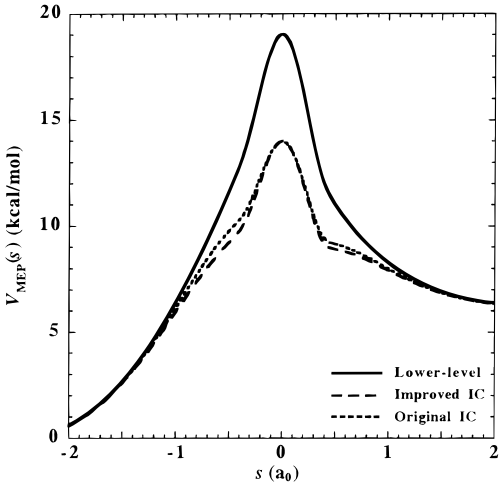

Figure 3. Born−Oppenheimer potential energy along the minimum-energy path for the PM3-SRP and PM3-SRP-IC surfaces, using two different schemes for the dual-level calculations.

of a bohr, but it appears to be unphysical at larger distances from the saddle point.

On the basis of these observations, we propose to use the original method in those cases for which a very small correction in the energy is required and the improved method elsewhere. In the rest of the paper we will use the original method for the dual-level calculations based on the APS and the improved method for the dual-level calculations based on the PM3-SRP surface.

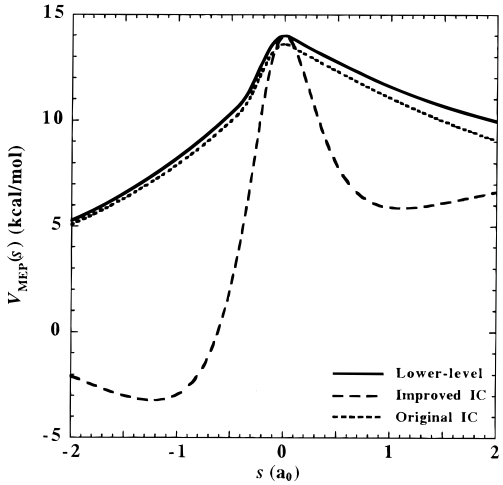

Figure 4. Born−Oppenheimer potential energy along the minimum-energy path for the APS and APS-IC surfaces, using two different schemes for the dual-level calculations.

As mentioned above, we use both the ICA[2] and ICL[3] algorithms for correcting the frequencies, and we use redundant curvilinear coordinates for vibrational analysis. To demonstrate the importance of using a curvilinear treatment of the vibrations, we performed some calculations using rectilinear coordinates as well. We found that the use of rectilinear coordinates sometimes leads to imaginary frequencies along the reaction path. These imaginary frequencies are not due to ridges or bifurcations on the surface, but rather to the unphysicality of rectilinear coordinates.[4,5,59,70] When the vibrations are treated by using rectilinear coordinates, the frequencies of the two lowest modes become imaginary near the saddle point. This problem disappears when the vibrations are treated in curvilinear coordinates. In dual-level calculations employing rectilinear coordinates the effect of these imaginary frequencies can be reduced by directly interpolating the lowest-frequency modes by using the IVTST-0 approximation[52] instead of the ICA and ICL algorithms employed in the dual-level calculation of the remaining frequencies. Note that the IVTST-0 method is independent of whether curvilinear or rectilinear coordinates are used because it uses data only at stationary points where the two coordinate systems give identical results. The change from rectilinear to curvilinear coordinates in principle affects all the frequencies, but, as usual, the modes most dependent on the choice of coordinates are those with the lowest frequencies, especially the transitional modes that evolve into free rotations or translations at reactants and/or products. The magnitudes of the frequencies of these modes can have a large effect on

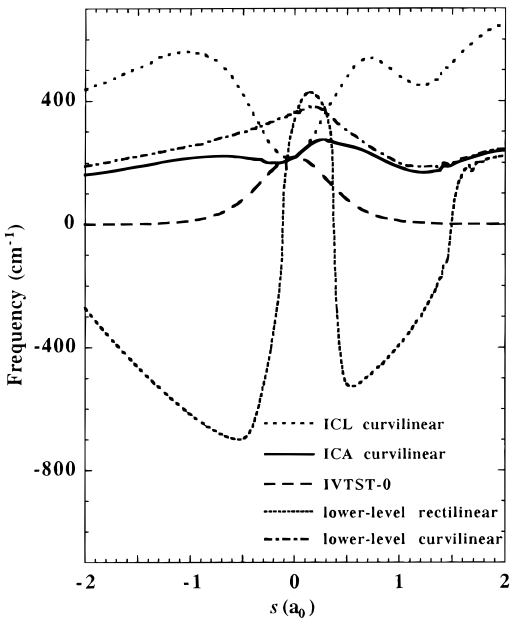

Figure 5. Frequencies of the lowest-frequency mode as given by the PM3-SRP surface in rectilinear and curvilinear coordinates, by the IVTST-0 approach, and by the two dual-level curvilinear calculations. Imaginary frequencies are plotted as negative numbers. The abcissa is the reaction coordinate.

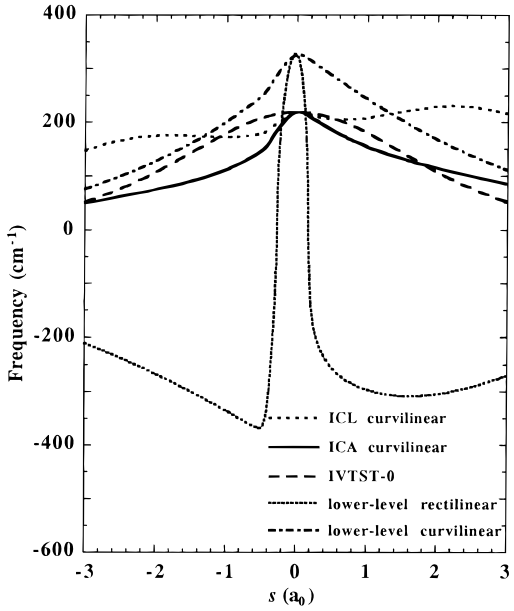

Figure 6. Frequencies of the lowest-frequency mode as given by the APS surface in rectilinear and curvilinear coordinates, by the IVTST-0 approach, and by the two dual-level curvilinear calculations. Imaginary frequencies are plotted as negative numbers. The abcissa is the reaction coordinate.

calculated rate constants. In fact, we found that if we treat the two lowest modes by using the IVTST-0 approach, the differences between the results obtained with rectilinear and curvilinear coordinates are about a factor of 1.5 in the final rate constants at 300 K, while the differences in a complete dual-level calculation with either curvilinear or rectilinear coordinates are larger than a factor of 5 at the same temperature.

A second check on the options for dual-level calculations is to compare the use of IVTST-0 interpolation for the lowest modes versus the use of dual-level curvilinear ICA and ICL methods. Figures 5 and 6 show the change along the reaction path of the lowest frequency using the IVTST-0 method and ICA and ICL methods with curvilinear coordinates. For comparison, we also show some results obtained with the lower-level surface, with both rectilinear and curvilinear coordinates. It has to be noted that for the APS lower-level the two lowest frequency modes are degenerate (the reaction path has C_{3v} symmetry). This degeneracy disappears after introducing the higher-level corrections, since two different higher-level frequencies are used to correct the lower-level double-degenerate frequencies. The PM3-SRP surface does not suffer this degeneracy, but the two lowest frequencies have very similar values.

In Figure 5 we can see that the IVTST-0 scheme is not very appropriate for the PM3-SRP surface. An IVTST-0 interpolation will always set the maximum of the frequency at the saddle point for a transitional mode, and the resulting frequency will be a symmetric function of the reaction coordinate since the value at both reactants and products is the same, namely zero. However the lower-level calculations show that the frequency is not a symmetric function of the reaction coordinate, and the maximum is located away from the saddle point. Thus, although the IVTST-0 method introduces significant improvement when undesired imaginary frequencies appear as a consequence of the use of rectilinear coordinates, it is not a good approximation to a full calculation in which the lowest frequencies are treated by means of curvilinear coordinates and they do not take imaginary values.

If we compare the results from ICA and ICL methods based on curvilinear coordinates, we can see that the ICL method shows an irregular behavior, with the frequencies increasing as we move out of the saddle point, then dropping again in order to reach their asymptotic values of zero at reactants and products. The ICA scheme, however, leads to a behavior more similar to the one observed in the lower-level surface, which seems more reasonable than the ICL behavior. The ICL method is designed to avoid the possible appearance of negative (not imaginary) frequencies along the reaction path that could show up when using the ICA scheme. However, it seems that the exponential dependence of the corrective function in this case leads to irregular changes of the corrected frequencies. Since the curvilinear ICA method does not have the problem of negative frequencies for the reaction studied here, the curvilinear ICA method will be selected for the rate constant calculations based on the PM3-SRP lower-level surface.

In Figure 6 we can see that the use of the APS lower level seems to give more consistent results. The IVTST-0, curvilinear ICL, and curvilinear ICA curves are more similar to each other, although once again the curvilinear ICA results seem to yield a shape closer to the lower-level calculations and a more regular behavior. Therefore, the curvilinear ICA scheme will also be used for the dual-level calculations based on the APS lower-level surface.

A third method denoted as interpolated-corrections-based-on-ratios[62] (ICR) has also been tested, yielding results similar to the original ICA formulation, giving more confidence to our choice of the ICA method for the study of the present reaction.

3.3. Rate Constants. Dual-level-calculated thermal forward rate constants for the $CH_4 + O(^3P)$ reaction at temperatures ranging from 300 to 2500 K are listed in Tables 7 and 8 and compared to the experimental measurements.[16,17,19] For comparison, single-level APS rate constants are given in Table S-3.

First we note the importance of the CUS[53,54] correction. For the PM3-SRP-based calculation this correction is more important at lower temperatures. The reason is that $\Delta G^{GT,0}$ has two maxima that become more similar to one another as the

TABLE 7: PM3-SRP−IC Rate Constants (in cm^3 molecule^{-1} s^{-1}) for $CH_4 + O(^3P)$

T (K)	TST	CVT	CUS	CUS/SCT	CUS/μOMT	expt[a]	expt[b]
300	9.96(−19)[c]	8.02(−19)	4.52(−19)	2.15(−18)	1.05(−17)	9.01(−18)	5.54(−18)
400	8.71(−17)	7.40(−17)	4.31(−17)	9.92(−17)	1.82(−16)	3.45(−16)	3.04(−16)
500	1.42(−15)	1.18(−15)	7.33(−16)	1.22(−17)	1.60(−15)	3.44(−15)	3.65(−15)
600	9.88(−15)	7.65(−15)	5.20(−15)	7.35(−15)	8.50(−15)	1.72(−14)	2.01(−14)
1000	6.93(−13)	3.93(−13)	3.46(−13)	3.89(−13)	4.02(−13)	6.01(−13)	7.69(−13)
1500	8.31(−12)	3.47(−12)	3.47(−12)	3.65(−12)	3.70(−12)	5.02(−12)	6.01(−12)
2000	3.44(−11)	1.17(−11)	1.12(−11)	1.16(−11)	1.16(−11)	1.76(−11)	1.92(−11)
2500	8.88(−11)	2.60(−11)	2.50(−11)	2.54(−11)	2.56(−11)	4.21(−11)	4.17(−11)

[a] Values from Cohen (ref 17). [b] Values from Klemm and Baulch and their co-workers (refs 16 and 19). [c] 9.96(−19) stands for 9.96×10^{-19}.

TABLE 8: APS−IC Rate Constants (in cm^3 molecule^{-1} s^{-1}) for $CH_4 + O(^3P)$

T (K)	TST	CVT	CUS	CUS/SCT	CUS/μOMT	expt[a]	expt[b]
300	9.96(−19)[c]	2.20(−19)	2.20(−19)	5.79(−19)	1.02(−17)	9.01(−18)	5.54(−18)
400	8.71(−17)	2.78(−17)	2.62(−17)	4.58(−17)	3.38(−16)	3.45(−16)	3.04(−16)
500	1.42(−15)	5.55(−16)	5.11(−16)	7.33(−16)	3.21(−15)	3.44(−15)	3.65(−15)
600	9.88(−15)	4.37(−15)	3.96(−15)	5.07(−15)	1.58(−14)	1.72(−14)	2.01(−14)
1000	6.93(−13)	3.72(−13)	3.15(−13)	3.42(−13)	5.61(−13)	6.01(−13)	7.69(−13)
1500	8.31(−12)	4.70(−12)	3.68(−12)	3.79(−12)	4.82(−12)	5.02(−12)	6.01(−12)
2000	3.44(−11)	1.96(−11)	1.44(−11)	1.46(−11)	1.68(−11)	1.76(−11)	1.92(−11)
2500	8.88(−11)	5.06(−11)	3.51(−11)	3.54(−11)	3.87(−11)	4.21(−11)	4.17(−11)

[a] Values from Cohen (ref 17). [b] Values from Klemm and Baulch and their co-workers (refs 16 and 19). [c] 9.96(−19) stands for 9.96×10^{-19}.

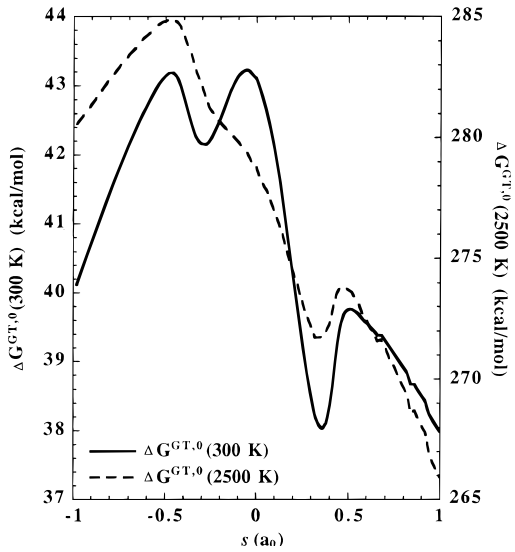

Figure 7. Generalized standard-state free energy of activation calculated at the PM3-SRP-IC level at 300 and 2500 K. The abcissa is the reaction coordinate.

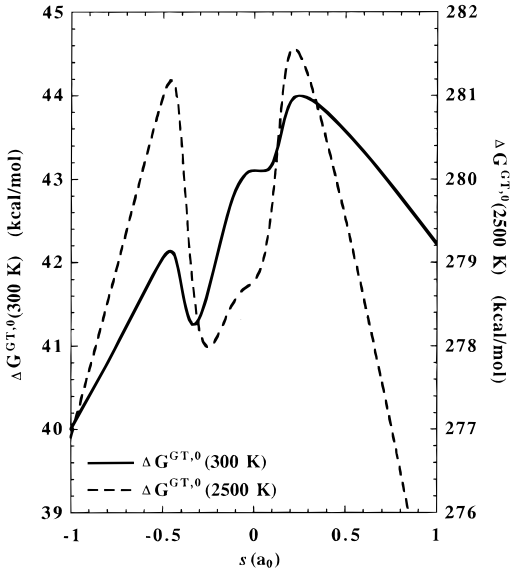

Figure 8. Generalized standard-state free energy of activation calculated at the APS-IC level at 300 and 2500 K. The abcissa is the reaction coordinate.

temperature decreases; this is illustrated in Figure 7. The CUS corrections are more important for a situation in which two maxima of similar height are separated by a deep minimum, which occurs for the $\Delta G^{GT,0}$ curve at lower temperatures, where two maxima at $s \approx 0$ and $s \approx -0.5\ a_0$ are present. At high temperatures, the maximum at $s \approx 0$ disappears, giving rise to a single maximum for the $\Delta G^{GT,0}$ profile. The APS-based calculations (Tables 8 and S-3 and Figure 8) show an opposite behavior, with an almost negligible CUS factor at low temperatures that increases as the temperature increases. The reason is an opposite behavior of the free energy of activation profile. At low temperatures one of the maxima dominates, but as we increase the temperature, a second maximum at $s \approx -0.5\ a_0$ becomes more important. Thus, at 2500 K two approximately equally high maxima in the $\Delta G^{GT,0}$ curve lead to a large CUS correction. (Our previous experience indicates that the unified statistical model may overestimate the correction to CVT. Nevertheless, the CUS method may be preferred to the CVT method because it leads to smooth curves of k versus T under general circumstances.)

For the APS lower level at 300 K, the ZCT tunneling factor is 1.8; the inclusion of the effects of reaction-path curvature by means of the SCT factor increases it only by about 50%, while the use of the LCT approach gives a factor of 46.4. This big difference between LCT and SCT tunneling leads to μOMT coefficients almost equal to the LCT ones. These values imply that tunneling occurs mainly in the extended part of the reaction swath, that is, in the nonadiabatically accessible region on the concave side of the reaction path. This can occur when the shortening of the path by cutting through the swath is significant enough to overcome the fact that the barrier is higher there.

In Table 9 are listed the values of the activation energies in five different temperature ranges, in each case calculated by a two-point fit at the extremes of the range. The calculated activation energies at the CVT/μOMT dynamical level are close

TABLE 9: Theoretical[a] and Experimental Activation Energies (kcal/mol)

method	300−400 K	400−500 K	500−900 K	900−1500 K	1500−2500 K
PM3-SRP−IC[b]	6.80	8.63	10.81	13.02	14.41
APS−IC[c]	8.35	8.94	10.10	12.51	15.53
APS	8.40	9.11	10.37	12.76	15.59
expt[d]	8.67	9.13	10.12	12.35	15.85
expt[e]	9.56	9.87	10.53	12.05	14.42

[a] Calculated using the CUS/μOMT rate constants. [b] PMP2-SAC/cc-pVTZ//UMP2/cc-pVTZ///PM3-SRP level. [c] PMP2-SAC/cc-pVTZ//UMP2/cc-pVTZ///APS level. [d] Values from Cohen (ref 17). [e] Values from Klemm and Baulch and their co-workers (refs 16 and 19).

to the experimental values, especially for the two calculations using the APS. The dual-level calculation based on the PM3-SRP surface seems to overestimate the tunneling contribution, leading to low activation energies at the lowest temperatures; this may result from $V_{MEP}(s)$ being too low on the product side, as seen in Figure 5. An important benefit of calculations such as those presented here is that they give us insight into which energetic questions deserve further study. In the present case we see that converging $V_{MEP}(s)$ on the product side with respect to electron-correlation level and basis set (a nontrivial task) would be very worthwhile.

Figure 9 shows the ratios of three sets of rate constants to the high-level conventional TST ones. The first set of results is our best theoretical result, CUS/μOMT at the PMP2-SAC/cc-pVTZ//UMP2/cc-pVTZ///APS level. The other two sets of results are the experimental results from refs 17 and 19. We see that our best theoretical calculation tracks extremely well with the results of ref 17, being about a factor of 10 bigger than TST at 300 K and a factor of 2.1−2.3 lower at 2500 K.

Finally, to make a quantitative estimation of the role of the tunneling in the curvature of the Arrhenius plots, we fitted our APS-IC results to a three-term expression of the type $AT^m \exp(-B/T)$. The resulting equation,

$$k = 6.96 \times 10^{-19}\, T^{2.46} \exp(-3410/T)\ \mathrm{cm^3\ molecule^{-1}\ s^{-1}} \quad (7)$$

shows a more pronounced curvature of the plot (bigger value of m) than the experimental measurements, although in reasonably good agreement with Cohen's expresion.[17] This behavior is more pronounced in the single-level APS ($m = 2.53$) and especially in the dual-level PM3-SRP-IC calculations ($m = 2.85$).

3.4. Kinetic Isotope Effects. Values of the theoretical kinetic isotope effect, defined as the ratio between the rate constants for the $CH_4 + O$ (Tables 7, 8, and S-3) and $CD_4 + O$ (Tables 10, 11, and S-4) reactions, are listed in Tables 12, 13, and S-5. Unfortunately, as far as we know, no experimentally determined isotope data are available for comparison.

It is interesting to note that for the $CD_4 + O$ reaction, with much lower tunneling contributions than the $CH_4 + O$ reaction, the SCT tunneling factor agrees better with the μOMT one. In the case of the dual-level calculation with the APS as the lower level, where LCT tunneling is more important, the SCT and μOMT transmission coefficients differ by a factor of 2.5, while in the calculation based on the PM3-SRP surface, the SCT contribution to the μOMT tunneling dominates for most of the energies. Another conclusion that can be drawn from the information in Tables 10, 11, and S-4 is that the CUS correction is not as important for the deuterated isotopomer as for the perprotio isotopomer.

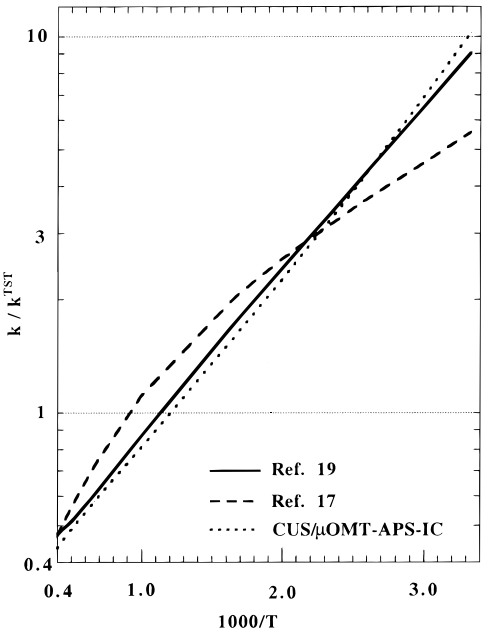

Figure 9. Ratios of rate constants to high-level TST rate constants. Dotted curve represents CUS/μOMT-APS-IC results, solid curve represents experiment from ref 19, and dashed curve represents results from ref 17.

TABLE 10: PM3-SRP−IC Rate Constants (in cm^3 molecule^{-1} s^{-1}) for $CD_4 + O(^3P)$

T (K)	TST	CVT	CUS	CUS/SCT	CUS/μOMT
300	9.74(−20)[a]	7.94(−20)	7.24(−20)	2.42(−19)	2.55(−19)
400	1.52(−17)	1.29(−17)	1.17(−17)	2.17(−17)	2.19(−17)
500	3.54(−16)	3.02(−16)	3.00(−16)	4.35(−16)	4.38(−16)
600	3.13(−15)	2.66(−15)	2.64(−15)	3.40(−15)	3.41(−15)
1000	3.47(−13)	2.18(−13)	2.14(−13)	1.88(−13)	1.89(−13)
1500	5.03(−12)	2.32(−12)	2.30(−12)	2.07(−12)	2.07(−12)
2000	2.25(−11)	8.62(−12)	8.54(−12)	7.84(−12)	7.85(−12)
2500	6.02(−11)	2.03(−11)	2.03(−11)	1.86(−11)	1.86(−11)

[a] 9.74(−20) stands for 9.74×10^{-20}.

TABLE 11: APS−IC Rate Constants (in cm^3 molecule^{-1} s^{-1}) for $CD_4 + O(^3P)$

T (K)	TST	CVT	CUS	CUS/SCT	CUS/μOMT
300	9.74(−20)[a]	7.02(−20)	6.81(−20)	1.38(−19)	3.50(−19)
400	1.52(−17)	1.20(−17)	1.18(−17)	1.75(−17)	2.82(−17)
500	3.54(−16)	2.91(−16)	2.88(−16)	3.69(−16)	4.90(−16)
600	3.13(−15)	2.63(−15)	2.61(−15)	3.09(−15)	3.72(−15)
1000	3.47(−13)	2.92(−13)	2.82(−13)	2.97(−13)	3.15(−13)
1500	5.03(−12)	4.14(−12)	3.76(−12)	3.84(−12)	3.94(−12)
2000	2.25(−11)	1.81(−11)	1.54(−11)	1.56(−11)	1.58(−11)
2500	6.02(−11)	4.77(−11)	3.84(−11)	3.87(−11)	3.90(−11)

[a] 9.74(−20) stands for 9.74×10^{-20}.

TABLE 12: PM3-SRP−IC Calculations of the H/D KIE for $CD_4 + O(^3P)$

T (K)	TST	CVT	CUS	CUS/SCT	CUS/μOMT
300	10.2	10.1	6.2	8.9	41.3
400	5.7	5.7	3.7	4.6	8.3
500	4.0	3.9	2.5	2.8	3.6
600	3.2	2.9	2.0	2.2	2.5
1000	2.0	1.80	1.61	2.07	2.1
1500	1.65	1.50	1.51	1.77	1.79
2000	1.53	1.35	1.31	1.47	1.48
2500	1.47	1.28	1.23	1.37	1.37

The calculated kinetic isotope effects (KIEs) for three methods are given in Tables 12, 13, and S-5; they show similar magnitudes and trends, but their values do not agree very well.

TABLE 13: APS−IC Calculations of the H/D KIE for the Reaction $CD_4 + O(^3P)$

T (K)	TST	CVT	CUS	CUS/SCT	CUS/μOMT
300	10.2	3.2	3.2	4.2	29.1
400	5.7	2.3	2.2	2.6	12.0
500	4.0	1.90	1.78	1.98	6.6
600	3.2	1.66	1.51	1.64	4.2
1000	2.0	1.27	1.12	1.15	1.78
2500	1.65	1.14	0.98	0.99	1.22
2000	1.53	1.08	0.93	0.94	1.06
2500	1.47	1.06	0.91	0.91	0.99

Thus, at 500 K, the μOMT KIE calculated using PM3-SRP as the lower level is only half of the value calculated using the APS as the lower-level surface. The agreement between the dual-level PMP2-SAC/cc-pVTZ//UMP2/cc-pVTZ///APS and single-level APS is better, but still not completely satisfactory. On the basis of the comparison with the perprotio rate data, we would take the dual-level calculation based on the APS as our best prediction.

4. Conclusions

In the present work we have studied the dynamics of the $CH_4 + O(^3P)$ reaction. We have determined the properties of reactants, products, and saddle point using accurate ab initio techniques that served as the higher level of a dual-level calculation. The dual-level calculation has been performed using two different lower levels: a semiempirical analytic surface and a direct dynamical PM3-SRP surface. The results are compared to experiment and also to single-level calculations on the analytic surface.

Several options for carrying out the dual-level calculations have been checked, and choices have been made according to the characteristics of the surfaces. The resulting dual-level calculations show reasonable agreement with each other, as well as with experimental results. The kinetic isotope effects (KIEs) are also calculated. Since no comparison is possible with experimental values for the KIEs, we have focused our attention on comparing the values obtained with the various levels. Once again, the agreement is not as good as observed in some other cases, but it is still reasonable.

The present work illustrates some pitfalls that dual-level dynamics calculations might encounter. It also shows the danger of using automatic procedures for dynamics calculation, which are strongly dependent on the properties of the reaction and characteristics of the surface and which, consequently, are hard to generalize.

From a different point of view, the present work tries to shed some light on an important combustion reaction that can be seen as a theoretical and experimental challenge. From a theoretical point of view, the challenge is due to the existence of two different potential energy surfaces and the Jahn−Teller effect. From an experimental point of view, the controversy about the stoichiometry of the reaction and the possibility of overestimated low-temperature rate constants is still open. The present calculations show that tunneling plays an important role in this reaction, and therefore, noticeable curvature in the Arrhenius plots can be expected.

Acknowledgment. The authors are grateful to Dr. E. Laura Coitiño and Mr. Patton L. Fast for their kind and helpful assistance. J.E.G. acknowledges the Junta de Extremadura (Spain) for a visiting professor scholarship. J.C.C. acknowledges a Fulbright fellowship which supported his stay at the University of Minnesota. O.R.N. thanks the Fundação de Amparo a Pesquisa do Estado de São Paulo (FAPESP) for a postdoctoral fellowship. This work was supported by the U.S. Department of Energy, Office of Basic Energy Sciences.

Supporting Information Available: Tables containing PM3-SRP and APS parameters, vibrational frequencies, and zero point energies for the $^3A''$ saddle point, and single-level rate constants and kinetic isotope effects based on the APS (5 pages). Ordering information is given on any current masthead page.

References and Notes

(1) (a) Tucker, S. C.; Truhlar, D. G. In *New Theoretical Concepts for Understanding Organic Reactions*; Bertrán, J., Csizmadia, I. G., Eds.; Kluwer: Dordrecht, The Netherlands, 1989; pp 291−346. (b) Truhlar, D. G.; Gordon, M. S. *Science* **1990**, *249*, 491. (c) Truhlar, D. G. In *The Reaction Path in Chemistry: Current Approaches and Perpectives*; Hedrich. D., Ed.; Kluwer: Dordrecht, The Netherlands, 1995; pp 229−255. (d) Truhlar, D. G.; Garrett, B. C.; Klippenstein, S. J. *J. Phys. Chem.* **1996**, *100*, 12771.

(2) Hu, W.-P.; Liu, Y.-P., Truhlar, D. G. *J. Chem. Soc., Faraday Trans.* **1994**, *90*, 1715.

(3) Chuang, Y.-Y.; Truhlar, D. G. *J. Phys. Chem. A* **1997**, *101*, 3808.

(4) (a) Jackels, C. F.; Gu, Z.; Truhlar, D. G. *J. Chem. Phys.* **1995**, *102*, 3188. (b) Chuang, Y.-Y.; Truhlar, D. G. *J. Chem. Phys.* **1997**, *107*, 83.

(5) Chuang, Y.-Y.; Truhlar, D. G. *J. Phys. Chem. A* **1998**, *102*, 242.

(6) (a) Morokuma, K.; Kato, S. In *Potential Energy Surfaces and Dynamics Calculations*; Truhlar, D. G., Ed.; Plenum: New York, 1981; pp 243−264. (b) Miller, W. H. *Ibid.*, pp 265−286. (c) Garrett, B. C.; Truhlar, D. G.; Grev, R. S. *ibid.*, pp 587−632.

(7) Hehre, W. J.; Radom, L.; Schleyer, P. v. R.; Pople, J. A. *Ab Initio Molecular Orbital Theory*; Wiley: New York, 1986.

(8) (a) Seifert, G.; Krüger, K. In *The Reaction Path in Chemistry: Current Approaches and Perpectives*; Heidrich, D., Ed., Kluwer: Dordrecht, The Netherlands, 1995; pp 229−255. (b) Truong, T. N.; Duncan, W. T.; Bell, R. L. In *Chemical Applications of Density Functional Theory*; Laird, B. B., Ross, R. B., Ziegler, T., Eds.; American Chemical Society: Washington, 1996; pp 85−104.

(9) Dewar, M. J. S.; Thiel, W. *J. Am. Chem. Soc.* **1977**, *98*, 4899.

(10) Dewar, M. J. S.; Zoebisch, E. G.; Healy, E. F.; Stewart, J. J. P. *J. Am. Chem. Soc.* **1985**, *107*, 3902.

(11) Stewart, J. J. P. *J. Comput. Chem.* **1989**, *10*, 221.

(12) (a) González-Lafont, A.; Truong, T. N.; Truhlar, D. G. *J. Phys. Chem.* **1991**, *95*, 4618. (b) Rossi, I.; Truhlar, D. G. *Chem. Phys. Lett.* **1995**, *233*, 231.

(13) (a) Truhlar, D. G.; Steckler, R.; Gordon, M. S. *Chem. Rev.* **1987**, *87*, 217. (b) Schatz, G. C. *Rev. Mod. Phys.* **1989**, *61*, 669.

(14) Warnatz, J. In *Combustion Chemistry*; Gardiner, W. C., Ed.; Springer-Verlag: New York, 1984; p 233.

(15) (a) Cadle, R. D.; Allen, E. R. *J. Phys. Chem.* **1965**, *69*, 1611. (b) Brown, J. M.; Thrush, B. A. *Trans. Faraday Soc.* **1967**, *63*, 630. (c) Wong, E. L.; Potter, A. E. *Can. J. Chem.* **1967**, *45*, 367. (d) Froben, F. W. *Ber. Bunsen-Ges. Phys. Chem.* **1968**, *72*, 996. (e) Westenberg, A. A.; De Haas, N. *J. Chem. Phys.* **1969**, *50*, 2512. (f) Herron, J. T. *Int. J. Chem. Kinet.* **1969**, *1*, 527. (g) Dean, A. M.; Kistiakowsky, G. B. *J. Chem. Phys.* **1971**, *54*, 1718. (h) Herron, J. T.; Huie, R. E. *J. Phys. Chem. Ref. Data* **1973**, *2*, 467. (i) Barassin, J.; Combourieu, J. *Bull. Soc. Chim. Fr.* **1974**, *1*, 1. (j) Roth, P.; Just, Th. *Ber. Bunsen-Ges. Phys. Chem.* **1977**, *81*, 572. (k) Shaw, R. *J. Phys. Chem. Ref. Data* **1978**, *7*, 1179. (l) Klemm, R. B.; Tanzawa, T.; Skolnik, E. G.; Michael, J. V. *18th Symp. (Int.) Combust.* **1981**, 785. (m) Fontijn, A. *18th Symp. (Int.) Combust.* **1981**, 797. (n) Tsang, W.; Hampson, R. F. *J. Phys. Chem. Ref. Data* **1986**, *15*, 1087. (o) Cohen, N.; Westberg, K. R. *Int. J. Chem. Kinet.* **1986**, *18*, 99.

(16) Baulch, D. L.; Cobos, C. J.; Cox, R. A.; Esser, P.; Frank, P.; Just, Th.; Kerr, J. A.; Pilling, M. J.; Troe, J.; Walker, R. W.; Warnatz, J. *J. Phys. Chem. Phys. Ref. Data* **1992**, *21*, 445.

(17) (a) Cohen, N. *Int. J. Chem. Kinet.* **1986**, *18*, 59. (b) Cohen, N.; Westberg, K. R. *Int. J. Chem. Kinet.* **1986**, *18*, 99.

(18) Herron, J. T. *J. Phys. Chem. Ref. Data* **1988**, *17*, 967.

(19) Sutherland, J. W.; Michael, J. V.; Klemm, R. B. *J. Phys. Chem.* **1986**, *90*, 5941.

(20) Westenberg, A. A.; De Haas, N. *J. Chem. Phys.* **1967**, *46*, 490.

(21) Brabbs, T. A.; Brokaw, R. S. *15th Symp. (Int.) Combust.* **1975**, 893.

(22) Walch, S. P.; Dunning, T. H. *J. Chem. Phys.* **1980**, *72*, 3221.

(23) Gonzalez, C.; McDonald, J. J. W.; Schegel, H. B. *J. Phys. Chem.* **1990**, *94*, 7467.

(24) (a) Møller, C.; Plesset, M. S. *Phys. Rev.* **1934**, *46*, 618. (b) Pople, J. A.; Seeger, R.; Krishnan, R. *Int. J. Quantum Chem. Symp.* **1977**, *11*, 149.

(25) (a) Garrett, B. C.; Truhlar, D. G.; Wagner, A. F.; Dunning, T. H., Jr. *J. Chem. Phys.* **1983**, *28*, 4400. (b) Kreevoy, M. M.; Ostovi, D.; Truhlar, D. G.; Garrett, B. C. *J. Phys. Chem.* **1986**, *90*, 3766. (c) Garrett, B. C.; Joseph, T.; Truong, T. N.; Truhlar, D. G. *Chem. Phys.* **1989**, *136*, 271.

(26) Liu, Y.-P.; Lu, D.-h.; González-Lafont, A.; Truhlar D. G.; Garrett, B. C. *J. Am. Chem. Soc.* **1993**, *115*, 7806.

(27) (a) Pople, J. A.; Nesbet, R. K. *J. Chem. Phys.* **1959**, *22*, 571. (b) Bartlett, R. J.; Purvis, G. D. *Int. J. Quantum Chem.* **1978**, *14*, 561.

(28) (a) McWeeny, R.; Diercksen, G. H. F. *J. Chem. Phys.* **1968**, *49*, 4852. (b) Lauderdale, W. J.; Stanton, J. F.; Gauss, J.; Watts, J. D.; Bartlett, R. J. *Chem. Phys. Lett.* **1991**, *187*, 21. (c) Lauderdale, W. J.; Stanton, J. F.; Gauss, J.; Watts, J. D.; Bartlett, R. J. *J. Chem. Phys.* **1992**, *97*, 6606.

(29) Hehre, W. J.; Ditchfield, R.; Pople, J. A. *J. Chem. Phys.* **1972**, *56*, 2257.

(30) Dunning, T. H., Jr. *J. Chem. Phys.* **1989**, *90*, 1007.

(31) (a) Löwdin, P.-O. *Phys. Rev.* **1955**, *97*, 1509. (b) Amos, T.; Hall, G. G. *Proc. R. Soc. London Ser. A* **1961**, *263*, 483. (c) Schlegel, H. B. *J. Chem. Phys.* **1986**, *84*, 4530. (d) Schlegel, H. B. *J. Chem. Phys.* **1988**, *92*, 3075. (e) Knowles, P. J.; Handy, N. C. *J. Phys. Chem.* **1988**, *92*, 3097. (f) Chen, W.; Schlegel, H. B. *J. Chem. Phys.* **1994**, *101*, 5957.

(32) (a) Cizek, J. *Adv. Chem. Phys.* **1969**, *14*, 35. (b) Purvis, G. D.; Bartlett, R. J. *J. Chem. Phys.* **1982**, *76*, 1910. (c) Pople, J. A.; Head-Gordon, M.; Raghavachari, K. *J. Chem. Phys.* **1987**, *87*, 5968. (d) Rittby, M.; Bartlett, R. J. *J. Phys. Chem.* **1988**, *92*, 3033. (e) Bartlett, R. J.; Watts, J. D.; Kucharski, S. A.; Noga, J. *Chem. Phys. Lett.* **1990**, *165*, 513. (f) Lee, T. J. Scuseria, G. E. In *Quantum Mechanical Electronic Structure Calculations with Chemical Accuracy*; Langhoff, S. R., Ed.; Kluwer: Dordrecht, The Netherlands, 1994. (g) Gauss, J.; Lauderdale, W. J.; Stanton, J. F.; Watts, J. D.; Bartlett, R. *Chem. Phys. Lett.* **1991**, *182*, 207.

(33) (a) Gordon, M. S.; Truhlar, D. G. *J. Am. Chem. Soc.* **1986**, *108*, 5412. (b) Gordon, M. S.; Truhlar, D. G. *Int. J. Quantum Chem.* **1987**, *31*, 81. (c) Gordon, M. S.; Nguyen, K. A.; Truhlar, D. G. *J. Phys. Chem.* **1989**, *93*, 7356. (d) Rossi, I.; Truhlar, D. G. *Chem. Phys. Lett.* **1995**, *234*, 64.

(34) Corchado, J. C.; Truhlar, D. G. In *Combined Quantum Mechanical and Molecular Mechanical Methods*; Gao, J., Thompson, M. A., Eds.; Am. Chem. Soc. Symposium Series, to be published, and references therein.

(35) Frisch, M. J.; Trucks, G. W.; Schlegel, H. B.; Gill, P. M. W.; Johnson, B. G.; Robb, M. A.; Cheeseman, J. R.; Keith, T.; Petersson, G. A.; Montgomery, J. A.; Raghavachari, K.; Al-Laham, M. A.; Zakrzewski, V. G.; Ortiz, J. V.; Foresman, J. B.; Ciolowski, J.; Stefanov, B. B.; Nanayakkara, A.; Challacombe, M.; Peng, C. Y.; Ayala, P. Y.; Chen, W.; Wong, M. W.; Andres, J. L.; Replogle, E. S.; Gomperts, R.; Martin, R. L.; Fox, D. J.; Binkley, J. S.; Defrees, D. J.; Baker, J.; Stewart, J. J. P.; Head-Gordon, M.; Gonzalez, C.; Pople, J. A. *Gaussian 94*; Gaussian Inc.: Pittsburgh, 1995.

(36) Stanton, J. F.; Gauss, J.; Watts, J. D.; Lauderdale, W. J.; Bartlett, R. J. ACES II; University of Florida, Gainesville, 1994.

(37) (a) Schlegel, H. B. *J. Comput. Chem.* **1982**, *3*, 214. (b) Schlegel, H. B. In *New Theoretical Concepts for Understanding Organic Reactions*; Bertran, J., Ed.; Kluwer: The Netherlands, 1989; pp 33−53. (c) Peng, C. Y.; Ayala, P. Y.; Schlegel, H. B.; Frisch, M. J. *J. Comput. Chem.* **1996**, *17*, 49.

(38) Stewart, J. J. P.; Rossi, I.; Hu, W.-P.; Lynch, G. C.; Liu, Y.-P.; Truhlar, D. G. MOPAC, Version 5.07mn; University of Minnesota, Minneapolis, 1997.

(39) (a) Corchado, J. C.; Espinosa-García, J. *J. Chem. Phys.* **1996**, *105*, 3160. (b) Espinosa-García, J.; Corchado, J. C. *J. Chem. Phys.* **1996**, *105*, 3517. (c) Corchado, J. C.; Espinosa-García, J. *J. Chem. Phys.* **1997**, *106*, 4013. (d) Espinosa-García, J.; Corchado, J. C. *J. Phys. Chem.* **1997**, *101*, 7336.

(40) Espinosa-García, J.; Corchado, J. C. *J. Phys. Chem.* **1996**, *100*, 16561.

(41) Joseph, T.; Steckler, R.; Truhlar, D. G. *J. Chem. Phys.* **1987**, *87*, 7036.

(42) Jordan, M. J. T.; Gilbert, R. G. *J. Chem. Phys.* **1995**, *102*, 5669.

(43) *JANAF Thermochemical Tables*, Vol. 14, 3rd ed.; Chase, M. W., Davies, C. A., Downey, J. R., Frurip, D. J., McDonald, R. A., Syverud, A. N., Eds.; National Bureau of Standards: Washington, DC, 1985.

(44) Isaacson, A. D.; Truhlar, D. G. *J. Chem. Phys.* **1982**, *76*, 1380.

(45) Truhlar, D. G.; Kuppermann, A. *J. Am. Chem. Soc.* **1971**, *93*, 1840.

(46) Garrett, B. C.; Truhlar, D. G. *J. Phys. Chem.* **1979**, *83*, 1052, 1079.

(47) Fukui, K. In *The World of Quantum Chemistry*; Daudel, R., Pullman, A., Eds.; Reidel: Dordrecht, The Netherlands, 1974; pp 113−144.

(48) Ishida, K.; Morokuma, K.; Komornicki, A. *J. Phys. Chem.* **1977**, *66*, 2153.

(49) Page, M.; McIver, J. W., Jr. *J. Chem. Phys.* **1988**, *88*, 922.

(50) Gonzalez, C.; Schlegel, H. B. *J. Chem. Phys.* **1989**, *90*, 2154.

(51) Melissas, V. S.; Truhlar, D. G.; Garrett, B. C. *J. Chem. Phys.* **1992**, *96*, 5758.

(52) González-Lafont, A.; Truong, T. N.; Truhlar, D. G. *J. Chem. Phys.* **1991**, *95*, 8875.

(53) Truhlar, D. G., Isaacson, A. D., Garrett, B. C. In *The Theory of Chemical Reaction Dynamics*; Baer, M., Ed; CRC Press: Boca Raton, FL, 1985; Vol. 4, pp 65−137.

(54) Garrett, B. C.; Truhlar, D. G. *J. Chem. Phys.* **1982**, *76*, 1853.

(55) Miller, W. H. *J. Chem. Phys.* **1975**, *65*, 2216.

(56) (a) Herzberg, G. *Molecular Spectra and Molecular Structure. II. Electronic Spectra and Electronic Structure of Polyatomic Molecules*; Van Nostrand Reinhold: New York, 1966. (b) Bersuker, I. B. *The Jahn−Teller Effect and Vibronic Interactions in Modern Chemistry*; Plenum Press: New York, 1984.

(57) Lu, D.-h.; Truong, T. N.; Melissas, V. S.; Lynch, G. C.; Liu, Y.-P.; Garrett, B. C.; Steckler, R.; Isaacson, A. D.; Rai, S. N.; Hancock, G. C.; Lauderdale, J. G.; Joseph, T.; Truhlar, D. G. *Comput. Phys. Commun.* **1992**, *71*, 235.

(58) Truong, T. N.; Lu, D.-h.; Lynch, G. C.; Liu, Y.-P.; Melissas, V. S.; Stewart, J. J. P.; Steckler, R.; Garrett, B. C.; Isaacson, A. D.; González-Lafont, A.; Rai, S. N.; Hancock, G. C.; Joseph, T.; Truhlar, D. G. *Comput. Phys. Commun.* **1993**, *75*, 143.

(59) (a) Natanson, G. A.; Garrett, B. C.; Truong, T. N.; Joseph, T.; Truhlar, D. G. *J. Chem. Phys.* **1991**, *94*, 7875. (b) Nguyen, K. A.; Jackels, C. F.; Truhlar, D. G. *J. Chem. Phys.* **1996**, *104*, 6491.

(60) (a) Garrett, B. C.; Truhlar, D. G. *J. Chem. Phys.* **1979**, *70*, 1593. (b) Miller, W. H.; Handy, N. C.; Adams, J. E. *J. Chem. Phys.* **1980**, *72*, 99.

(61) Chuang, Y.-Y.; Fast, P. L.; Hu, W.-P.; Lynch, G. C.; Liu, Y.-P.; Truhlar, D. G. MORATE, Version 7.8; University of Minnesota, Minneapolis, 1997.

(62) Corchado, J. C.; Chuang, Y. Y.; Fast, P. L.; Coitiño, E. L.; Hu, W.-P.; Liu, Y.-P.; Lynch, G. C.; Nguyen, K. A.; Jackels, C. F.; Gu, M. Z.; Rossi, I.; Clayton, S.; Melissas, V. S.; Steckler, R.; Garrett, B. C.; Isaacson, A. D.; Truhlar, D. G. POLYRATE, Version 7.8; University of Minnesota, Minneapolis, 1997.

(63) Gaydon, A. G. *Dissociation Energies and Spectra of Diatomic Molecules*; Chapman and Hall: London, 1968.

(64) Head-Gordon, M. *J. Phys. Chem.* **1996**, *100*, 13213.

(65) Colt, J. R.; Scuseria, G. E. *Mol. Phys.* **1992**, *1099*, 75.

(66) Kreye, W. C. *Chem. Phys. Lett.* **1996**, *256*, 383.

(67) Brown, R. D. In *Structures and Conformations of Non-Rigid Molecules*; Laane, J., Dakkouri, M., van der Veken, B., Oberhammer, H., Eds.; Kluwer: Dordrecht, The Netherlands, 1993; pp 99−112.

(68) (a) Garrett, B. C.; Truhlar, D. G. *Theor. Chem. Adv. Perspect.* **1981**, *6A*, 215. (b) Mead, C. A.; Truhlar, D. G. *J. Chem. Phys.* **1979**, *20*, 2284.

(69) Corchado, J. C.; Espinosa-García, J.; Hu, W.-P.; Rossi, I.; Truhlar, D. G. *J. Phys. Chem.* **1995**, *99*, 687.

(70) Truhlar, D. G. *J. Chem. Soc., Faraday Trans.* **1994**, *90*, 1608.